PHYSICAL REVIEW B **89**, 180102(R) (2014)

# Tuning the crystal structure and electronic states of $Ag_2Se$: Structural transitions and metallization under pressure

Zhao Zhao,[1,2,*] Shibing Wang,[2,3] Artem R. Oganov,[4,5,6,*] Pengcheng Chen,[7,4] Zhenxian Liu,[8] and Wendy L. Mao[2,3,9]

[1]*Department of Physics, Stanford University, Stanford, California 94305, USA*

[2]*Stanford Institute for Materials and Energy Sciences, SLAC National Accelerator Laboratory, Menlo Park, California 94025, USA*

[3]*Department of Geological and Environmental Sciences, Stanford University, Stanford, California 94305, USA*

[4]*Department of Geosciences, Center for Materials by Design, and Institute for Advanced Computational Science, Stony Brook University, Stony Brook, New York 11794, USA*

[5]*Moscow Institute of Physics and Technology, Dolgoprudny city, Moscow Region 141700, Russian Federation*

[6]*Northwestern Polytechnical University, Xi'an 710072, China*

[7]*Department of Physics and State Key Laboratory of Low-Dimensional Quantum Physics, Tsinghua University, Beijing 100084, China*

[8]*Geophysical Laboratory, Carnegie Institution of Washington, Washington, D.C. 20015, USA*

[9]*Photon Science, SLAC National Accelerator Laboratory, Menlo Park, California 94025, USA*

(Received 22 November 2013; revised manuscript received 25 February 2014; published 22 May 2014)

We performed synchrotron x-ray diffraction and infrared (IR) experiments combined with evolutionary structure predictions and band structure calculations on $Ag_2Se$ to ~20 GPa. We present evidence for phase I ($\beta$-$Ag_2Se$) as a potential three-dimensional topological insulator by its increase in optical band gap and the topologically nontrivial nature of its band structure. Higher pressures induce a triple-layer stacking pattern and significantly increase the crystallographic inequivalence of the two Ag sites, where $P2_12_12_1$ phase I first reconstructs into a *Pnma* phase II, and then transforms into a topologically different *Cmcm* phase III. The radical changes in IR spectra and electronic band structures indicate the metallic nature of the high-pressure phases. Our results highlight the effects of pressure in tuning the crystal structure and electronic states of $Ag_2Se$.

DOI: 10.1103/PhysRevB.89.180102 PACS number(s): 61.50.Ks, 71.30.+h, 78.30.−j

In search of novel electronic states and spintronics materials, binary chalcogenides such as $Bi_2Se_3$ and $Bi_2Te_3$ have attracted great research interest since the discovery of three-dimensional (3D) topological insulators (TIs) [1–5]. For $Bi_2Se_3$ and $Bi_2Te_3$, the surface Dirac cones are highly symmetric as determined by their high symmetry hexagonal crystal structures. In contrast to isotropic TIs, anisotropic TIs possessing highly anisotropic cones lead to dramatically different physics such as spin conduction and charge transport [6,7]. Thus, new TIs with relatively low symmetry crystal structures are worth investigating.

$Ag_2Se$ belongs to the family of silver chalcogenides $Ag_2E$ ($E$ = S, Se, and Te). At elevated temperatures, they change from semiconducting $\beta$ phases to high temperature superionic $\alpha$ phases [8–18]. Nonstoichiometric $\beta$-$Ag_2Se$ and $\beta$-$Ag_2Te$ have potential applications in producing high-sensitivity magnetic sensors, due to the large linear magnetoresistance (LMR) observed over a wide range of magnetic fields and temperatures [19–22]. For explanations, classical [21,23,24] and quantum [25,26] theories based on the assumption of zero-gap semiconductors had been proposed. Recently, $\beta$-$Ag_2Te$ was predicted to be a new 3D TI with a highly anisotropic Dirac cone, and similar calculations showed $\beta$-$Ag_2Se$ was also topologically nontrivial [27]. The LMR in $\beta$-$Ag_2Se$ and $\beta$-$Ag_2Te$ could be induced by the two-dimensional (2D) metallic surface states [27], and experimental evidence for metallic surface states has been found in $\beta$-$Ag_2Te$ nanowires and nanoribbons [28,29]. To date, no related study on $\beta$-$Ag_2Se$ has been presented.

$\beta$-$Ag_2Se$ has a narrow band gap tunable via dimensionality, for example via film thickness and particle size [30–33]: with increasing film thickness, $Ag_2Se$ thin films exhibit larger activation gaps but lower electric resistivity [30]; IR spectra and optical band gaps in $Ag_2Se$-based quantum dots (nanoparticles) show a strong particle size dependence [31–33]. Pressure can provide another route to tune the electronic properties of $Ag_2Se$. Previous high-pressure studies on $Ag_2Te$ [34–37] and $Ag_2S$ [38,39] showed they have rich phase diagrams. For $Ag_2Te$, it was found that pressure effectively eliminates the LMR and alters the band structure [35], related to transitions from the insulating phase I to a semimetallic phase II, and then to a fully metallic phase III [36]. For $Ag_2S$, several structural transitions were identified below 18 GPa [38], and a recent high-pressure study combining electrical transport measurements with electronic structure calculations showed that its band gap decreases without full closure under compression [39].

For $Ag_2Se$, the only previous high-pressure study was reported nearly five decades ago, and the $\beta$ phase to $\alpha$ phase boundary was determined through temperature-dependent electric transport measurements up to about 5 GPa [40,41]. To further study the high-pressure behavior of $Ag_2Se$, we conducted room temperature *in situ* synchrotron x-ray diffraction (XRD) and IR experiments and performed evolutionary crystal structure prediction and theoretical band structure calculations. In this Rapid Communication, we present evidence for phase I being a 3D TI and report the discovery of metallic high-pressure phases.

The $Ag_2Se$ sample was purchased from Sigma-Aldrich. *In situ* angle dispersive XRD data was collected at 16 BM-D of the Advanced Photon Source (APS), Argonne National

*Corresponding authors: zhaozhao@stanford.edu; artem.oganov@sunysb.edu

 

Laboratory (ANL), and neon was used as the pressure transmitting medium. The Rietveld fitting was performed by the GSAS and EXPGUI package [42]. High-pressure IR measurements were conducted in beamline U2A of the National Synchrotron Light Source (NSLS), Brookhaven National Laboratory (BNL) and KBr was used as the pressure medium. Both reflectance and transmittance were measured in the spectral range between 600 and 8000 $cm^{-1}$ with a resolution of 4 $cm^{-1}$. The spectra normalization follows the procedures of a previous IR work [43].

To determine high-pressure structures, we used the evolutionary crystal structure prediction method USPEX [44–46], which has been successfully used in many earlier works [47–51]. Predictions were performed at ambient pressure, 13, 20, and 30 GPa. Structure relaxations and enthalpy calculations were performed using the VASP code [52] at the level of the generalized gradient approximation [53] in conjunction with the all-electron projector augmented-wave method. Brillouin zone integration was conducted with Γ-centered uniform meshes with resolution $2\pi \times 0.04$ $Å^{-1}$ and $2\pi \times 0.02$ $Å^{-1}$ for structural optimization and band structure calculation, respectively. Wave functions were expanded in plane waves with a kinetic energy cutoff of 340 eV. The spin-orbit coupling (SOC) was also included in the self-consistent calculations of the electronic structure.

XRD patterns collected during compression are shown in Fig. 1(a) (decompression patterns are shown in the Supplemental Material, Fig. S1 [54]). The transformation of phase I into a new phase II started at 7.8 GPa and completed at 10.6 GPa. From phase II to phase III (transition pressure ~16.5 GPa), though no new diffraction peaks appeared, some of the peaks [see the insets of Fig. 1(a)] shifted to smaller $2\theta$ (larger $d$ spacing). Phase III was stable up to the highest pressure 19.6 GPa in this study. Decompression data indicates all structural transitions were reversible: Phase III transformed back to phase II at 17.0 GPa, and then to phase I between 3.4 and 2.1 GPa [54].

At ambient conditions [see Fig. 2(d)], $\beta$-$Ag_2Se$ (phase I) has an orthorhombic structure ($P2_12_12_1$, $Z = 4$) [18], correctly predicted as the most stable structure by our USPEX calculations. High-pressure USPEX calculations yielded two similar orthorhombic structures as the two most stable (lowest enthalpy) structures (Fig. 2): a *Pnma* structure and a *Cmcm* structure [54]. At a lower pressure of 13 GPa, the *Pnma* structure has the lowest enthalpy, while at the higher pressures of 20 and 30 GPa the *Cmcm* structure has the lowest enthalpies. Our calculations also showed that this first-order transition occurs at around 18 GPa, close to the experimental result of 16.5 GPa [54]. To fully match the experimental XRD patterns in phase II and phase III, a metastable phase needs to be added into the Rietveld refinements (see Supplemental Material, Figs. S4 and S5 [54]). Two phases of Rietveld refinement results based on *Pnma* (*Cmcm*) and the fifth lowest energy $C2/m$ structures showed that the $C2/m$ has ~10% in weight. The metastable phase disappeared when decompressed to 5.2 GPa [see Supplemental Material, Figs. S1 and S4(a)]. Kinetic factors or deviatoric stresses may be responsible for the appearance of this metastable phase as the energy of the $C2/m$ structure is only ~0.001 eV/atom higher than those of the *Pnma* and *Cmcm* structures (Supplemental Material Table S3).

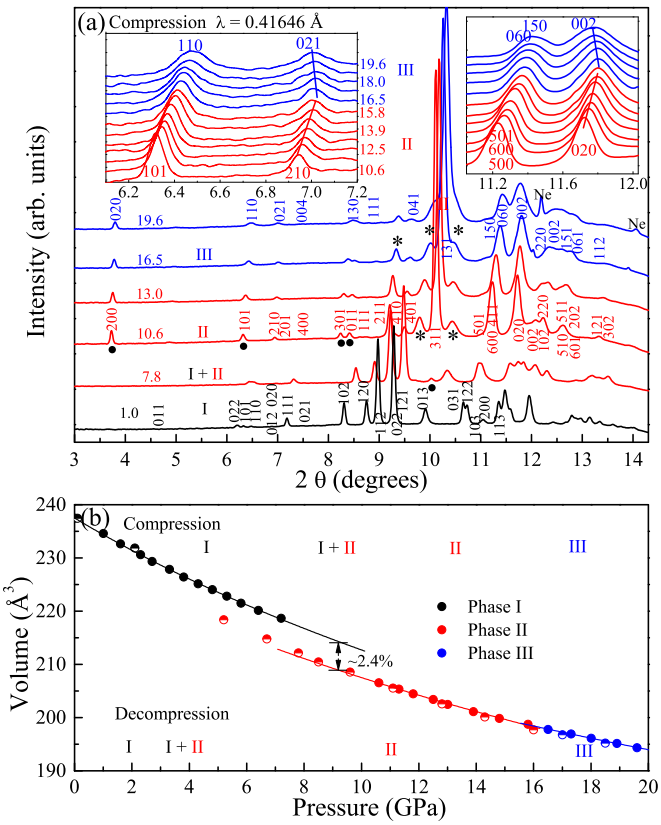


FIG. 1. (Color online) (a) Representative XRD patterns collected during the compression cycle. The circles marks new diffraction peaks from phase II. The asterisks are peaks not explainable by the first lowest energy structure from USPEX. The insets show that some diffraction peaks shift to larger $d$ spacing. (b) EOS of $Ag_2Se$; the full and half-filled circles are experimental data collected during the compression and decompression cycles, respectively.

Detailed comparisons of experiments and theories, single-phase and two-phase Rietveld refinements, and structures of metastable phases are provided in the Supplemental Material [54].

The equation of state (EOS) together with the phase diagram is shown in Fig. 1(b), where only the compressional data was used for EOS fitting. For phase I, a third-order Birch-Murnaghan EOS was used; $V_0$ was fixed at the experimental value of 237.5 $Å^3$. For phase I, the fitting yielded $B_0 =$ 73.5(11) GPa and $B' = 3.8(4)$. For phase II and phase III, a second-order Birch-Murnaghan was employed, as limited by the number of data points. For phase II, $V_0 = 229.2(7)$ $Å^3$ and $B_0 = 83(3)$ GPa; for phase III, $V_0 = 223.0(7)$ $Å^3$ and $B_0 = 108(3)$ GPa. Linear least-square of a finite-strain EOS $G$-$g$ fitting [55–57] yielded similar results.

Figure 2 shows the evolution of normalized cell parameters and crystal structures for all three phases. Phase I has a relatively low symmetry orthorhombic structure $P2_12_12_1$ without inversion symmetry [Fig. 2(d)] [18]. In between the Se layers, there are two Ag atoms where Ag1 lies closer to one Se layer and Ag2 is in between the layers. The cell parameter $a$ reflects one nearest Se-Se distance that decreases less than 0.5% [Fig. 2(a)]. Along the $c$ direction, the zigzag Se pattern experiences the largest shrinkage (about 4%), resulting from

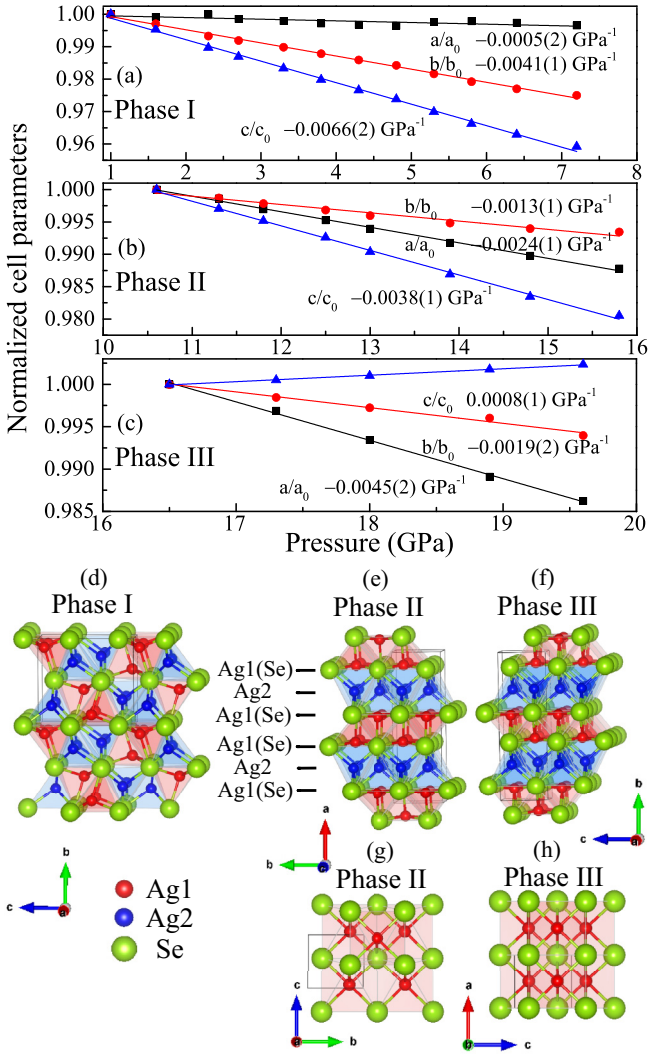


FIG. 2. (Color online) Evolution of normalized cell parameters with increasing pressure for (a) phase I, (b) phase II, and (c) phase III. (d)–(f) Structures of phases I, II, and III. Phase II and phase III exhibit Se(Ag1)-Ag2-Se(Ag1), a triple-layered stacking pattern. (g) and (h) highlight the structural difference between phase II and phase III.

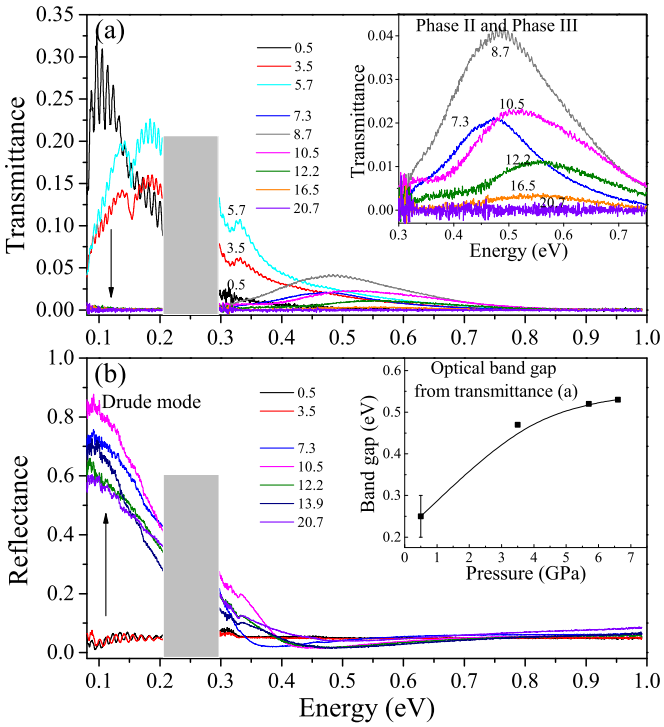


FIG. 3. (Color online) High-pressure IR (a) transmittance and (b) reflectance spectra for $Ag_2Se$ with increasing pressure. The 0.2–0.3 eV region is obscured by diamond absorption. The inset of (a) shows the distinctive transmission region for phase II and phase III, and the inset of (b) shows the band gap from the transmittance.

the large decrease in the nearest Se-Ag distances. In the *b* direction, the Se layer-nearby Se layer distances are almost equivalent. Clearly, pressure first decreases the nearest Se-Ag distances much more than the nearest Se-Se distances.

Further compression eventually reduces the Se-Se distances, and thus destabilizes the structure of phase I. From $P2_12_12_1$ phase I to *Pnma* phase II, a large structural reconstruction and a 2.4% volume drop were observed [Fig. 1(b)]. However, instead of undergoing uniform shrinkage in Se-Se distances, the Se layer pairs with one nearby Se layer and a triple-layered Se(Ag1)-Ag2-Se(Ag1) pattern forms along the *a* direction. Space group *Pnma* has the inversion symmetry, and its inversion center is located in between the adjacent Se(Ag1)-Ag2-Se(Ag1) triple layers. In the interlayer, the *c* axis is the most compressible and the *b* axis is the least compressible. From phase II to phase III, the inversion symmetry and inversion center are preserved. The higher symmetry *Cmcm* phase III [Fig. 2(f)] has cell parameters and triple layers similar to phase II. Yet these two structures are topologically different: the coordination of Ag1 with nearby Se increases from a fivefold pyramid [phase II, Fig. 2(g)] to a sixfold triangular prism [phase III, Fig. 2(h)], even though the Ag2 and nearby Se remain in a fourfold tetrahedra. The shifting of a few peaks to larger *d* spacings with pressure [Fig. 1(a)] corresponds to the elongation of the *c* axis, mostly related to the increasing ionic interactions in the Ag1. The enhanced anisotropy in the *ac* plane prevents the formation of a tetragonal lattice, despite cell parameter *c* being only about 7% larger than *a*. Compared with previous structural studies on $Ag_2Te$ [36] and $Ag_2S$ [38], $Ag_2Te$ phase III (*Cmca*) can be regarded as an in-plane doubled cell of $Ag_2Se$ phase II (*Pnma*) and phase III (*Cmcm*), while $Ag_2S$ phase II is isostructural with $Ag_2Se$ phase I ($P2_12_12_1$) and $Ag_2S$ phase III has a relatively low monoclinic symmetry ($P2_1/n$). Interestingly, $Ag_2S$ phase IV was also proposed to have a *Pnma* space group, yet its structure (for example, the cell parameters) was significantly different from $Ag_2Se$ phase II (*Pnma*).

To study the electronic behavior of $Ag_2Se$ under pressure, we performed IR measurements with photon energy 0.08–1 eV (Fig. 3) and band structure calculations (Fig. 4). At ambient conditions, $\beta$-$Ag_2Se$ is known as a narrow band gap semiconductor. The experimental optical band gap or activation energy ranged from 0.03 to 0.2 eV, depending on many factors such as homogeneity and film thickness [12,30,58,59]. With 2% transmittance defined as the cutoff of the optical band gap [60], the gap energy increases with pressure [see the inset of Fig. 3(b)],

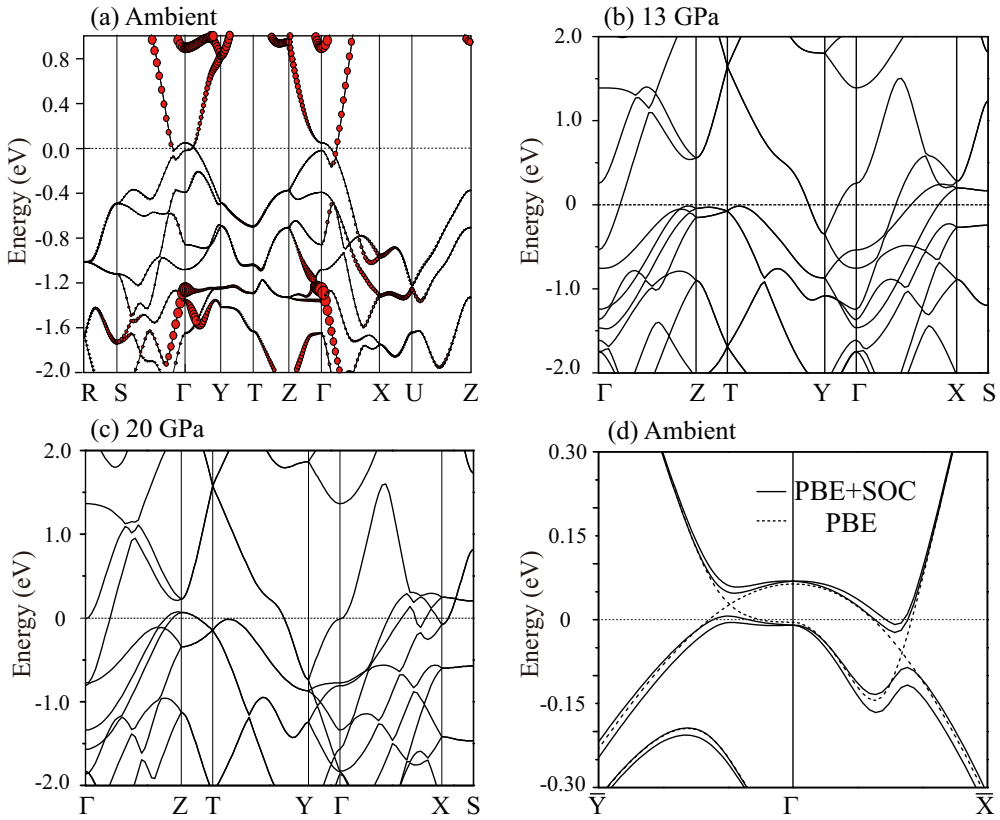


FIG. 4. (Color online) Calculated band structures for (a) phase I at ambient conditions (with SOC, the red dots show the Ag *s* orbital), (b) phase II at 13 GPa, (c) phase III at 20 GPa, and (d) detailed band structure of phase I near the Fermi level.

which appears to contradict the general compression picture. To explain this unexpected increase, we calculated the band structure at ambient pressure. In Fig. 4(a), phase I's topological nontrivial inverted band structure can be observed [27]. Among previously studied 3D topological insulators, the pressure induced band gap increase was only observed in $Bi_2Se_3$ [60,61]. On the basis that $\beta$-$Ag_2Se$ is indeed a semiconductor, this increase then marks its unusual electronic evolution as a potential 3D TI. The band inversion feature may enlarge the band gap around the Γ point (related to the only electric-dipole-allowed transition for photons) under compression [60].

It is worth noting that our Perdew-Burke-Ernzerhof (with and without SOC) and quasiparticle GW calculations, together with earlier reported local spherical wave calculations [62] produced metallic electronic structures at ambient conditions, different from early experimental evidence for a narrow gap semiconductor [30–33]. We found the SOC induced the metal to semimetal transition for $\beta$-$Ag_2Se$ [see Fig. 4(d)] [63]. SOC breaks the degeneracy of the crossing points near the Fermi level and opens the semimetallic gap. Admittedly, the existing computational methods may need to be improved to precisely describe the electronic structure of $Ag_2Se$. Yet our results clearly demonstrate the possibility of 2D metallic surface states, and this would require a reinterpretation of previous experimental data [30–33] and an update of previous theories [21,23–26].

When entering phase II above 7.3 GPa, the transmittance and reflectance spectra transform totally: no transmission was seen in the low energy region (0.86–0.3 eV) and a Drude mode appeared in the reflectance, indicating the metallic natures of phase II and phase III (the major phases contributed the most to the spectra). We calculated the band structures for phase II (*Pnma*) at 13 GPa [Fig. 4(b)] and phase III (*Cmcm*) at 20 GPa [Fig. 4(c)]. Both Fermi surfaces are relatively isotropic. Compared to the band structure at 13 GPa (*Pnma*), the result at 20 GPa (*Cmcm*) is more broadened and contributes more density of states around the Fermi level, leading to the enhancement of metallic states. For $Ag_2Te$, bulk metallic states were also obtained under high pressure [36,37], while for $Ag_2S$, its band gap decreased strongly without fully closing [39]. Clearly, the effects of different chalcogenide cations need to be distinguished in order to fully understand the structural and electronic behavior.

Our optical results demonstrated that $Ag_2Se$ processes a highly tunable IR transmission window as a function of pressure. We observed an abnormal mid-IR transmission in between 7.3 and 16.5 GPa corresponding to the metallic phase II region. A transmission window lies in the mid-IR region around 0.5 eV [inset of Fig. 3(a)] with systematic shifting to higher energy as the increase of pressure. This partial transmission could originate from the intraband features of the triple-layered phase II. At 20.7 GPa in the phase III region, pressure effectively closes the IR transmission window, as a proof for fully metallic phase III. The tunable distinctive IR transmission window may be applicable for pressure calibration at below 20 GPa. Considering the bulk metallic features of phase II and phase III, it is unnecessary to discuss its band topological nature. After the transition from 2D

surface metallic states conduction to 3D bulk metallic states conduction, the LMR is expected to vanish and the quadratic behavior will take over, based on conventional band theory with a closed Fermi surface [64].

In summary, we studied the high-pressure behavior of $Ag_2Se$ up to 20.7 GPa through a series of experiments and calculations and found pressure plays a dramatic role in tuning its structural and electronic properties. The ambient phase of $\beta$-$Ag_2Se$ may be a new anisotropic 3D topological insulator, as evidenced by the unusual increase in its optical band gap and its topologically nontrivial inverted band structure. At high pressures, its crystal structure reconstructed into a largely metallic phase II at 7.8 GPa where a distinctive Se(Ag1)-Ag2-Se(Ag1) triple-layer stacking pattern appeared, and then transformed to a completely metallic phase III at 16.5 GPa. Our results also suggest the existence of a small amount of a metastable phase with a monoclinic $C2/m$ structure. The electronic band calculations explained the evolution of IR spectra with pressure. The wide stability range of the multilayered high-pressure phases, their tunable IR properties, and expectable magneto response opens up the opportunity to design complex multifunctional materials under pressure.

We thank Arianna Gleason and beamline scientists Changyong Park and Sergey N. Tkachev for their assistance. Z.Z. is supported through the Stanford Institute for Materials and Energy Sciences by the Department of Energy (DOE), Office of Basic Energy Sciences (BES), Contract No. DE-AC02-76SF00515. S.W. is supported by EFree, an Energy Frontier Research Center funded by the U.S. DOE, BES, Grant No. DE-SG0001057. The work of A.R.O. is supported by the National Science Foundation (Grants No. EAR-1114313 and No. DMR-1231586), DARPA (Grants No. W31P4Q1310005 and No. W31P4Q1210008), the Government (Grant No. 14.A12.31.0003) and the Ministry of Education and Science of Russian Federation (Project No. 8512), and Foreign Talents Introduction and Academic Exchange Program (Grant No. B08040). P.C. thanks the exchange student fund of Tsinghua University for supporting his visit at Stony Brook University. Calculations were performed on XSEDE facilities and on the cluster of the Center for Functional Nanomaterials, BNL, supported by the DOE-BES, Contract No. DE-AC02-98CH10086. HPCAT operations are supported by DOE-NNSA Contract No. DE-NA0001974 and DOE-BES Contract No. DE-FG02-99ER45775, with partial instrumentation funding by NSF MRI-1126249. APS is supported by DOE-BES, under Contract No. DE-AC02-06CH11357. U2A is supported by COMPRES under NSF Cooperative Agreement EAR 11-57758 and DOE/NNSA (Contract No. DE-FC03-03N00144, CDAC). NSLS is supported by the DOE/BES (Contract No. DE-AC02-98CH10886).

[1] H. Zhang, C.-X. Liu, X.-L. Qi, X. Dai, Z. Fang, and S.-C. Zhang, Nat. Phys. **5**, 438 (2009).
[2] Y. L. Chen, J. G. Analytis, J.-H. Chu, Z. K. Liu, S.-K. Mo, X. L. Qi, H. J. Zhang, D. H. Lu, X. Dai, Z. Fang, S. C. Zhang, I. R. Fisher, Z. Hussain, and Z.-X. Shen, Science **325**, 178 (2009).
[3] Y. Xia, D. Qian, D. Hsieh, L. Wray, A. Pal, H. Lin, A. Bansil, D. Grauer, Y. S. Hor, R. J. Cava, and M. Z. Hasan, Nat. Phys. **5**, 398 (2009).
[4] D. Hsieh, Y. Xia, D. Qian, L. Wray, F. Meier, J. H. Dil, J. Osterwalder, L. Patthey, A. V. Fedorov, H. Lin, A. Bansil, D. Grauer, Y. S. Hor, R. J. Cava, and M. Z. Hasan, Phys. Rev. Lett. **103**, 146401 (2009).
[5] W. Zhang, R. Yu, H.-J. Zhang, X. Dai, and Z. Fang, New J. Phys. **12**, 065013 (2010).
[6] F. Virot, R. Hayn, M. Richter, and J. van den Brink, Phys. Rev. Lett. **106**, 236806 (2011).
[7] V. E. Sacksteder, S. Kettemann, Q. S. Wu, X. Dai, and Z. Fang, Phys. Rev. B **85**, 205303 (2012).
[8] P. Rahlfs, Z. Phys. Chem. B **51**, 157 (1935).
[9] R. Junod, Helv. Phys. Acta **32**, 581 (1959).
[10] *Superionic Conductors*, edited by G. D. Mahan and W. L. Roth (Plenum, New York, 1976).
[11] S. Miyatani, J. Phys. Soc. Jpn. **13**, 341 (1958).
[12] R. Dalven and R. Gill, J. Appl. Phys. **38**, 753 (1967).
[13] C. R. Veale, J. Less-Common Met. **11**, 50 (1966).
[14] F. Grønvold and E. Westrum, J. Chem. Thermodyn. **18**, 381 (1986).
[15] B. H. Grier, S. M. Shapiro, and R. J. Cava, Phys. Rev. B **29**, 3810 (1984).
[16] M. Fujikane, K. Kurosaki, H. Muta, and S. Yamanaka, J. Alloy. Compd. **393**, 299 (2005).
[17] A. Van der Lee and J. L. de Boer, Acta Crystallogr., Sect. C: Cryst. Struct. Commun. C **49**, 1444 (1993).
[18] J. Yu and H. Yun, Acta Crystallogr., Sect. E: Struct. Rep. Online **67**, i45 (2011).
[19] R. Xu, A. Husmann, T. F. Rosenbaum, J. E. Enderby, and P. B. Littlewood, Nature (London) **390**, 57 (1997).
[20] A. Husmann, J. B. Betts, G. S. Boebinger, A. Migliori, T. F. Rosenbaum, and M.-L. Saboungi, Nature (London) **417**, 421 (2002).
[21] M. M. Parish and P. B. Littlewood, Nature (London) **426**, 162 (2003).
[22] M. von Kreutzbruck, G. Lembke, B. Mogwitz, C. Korte, and J. Janek, Phys. Rev. B **79**, 035204 (2009).
[23] J. Hu, T. F. Rosenbaum, and J. B. Betts, Phys. Rev. Lett. **95**, 186603 (2005).
[24] J. Hu, M. M. Parish, and T. F. Rosenbaum, Phys. Rev. B **75**, 214203 (2007).
[25] A. A. Abrikosov, Phys. Rev. B **58**, 2788 (1998).
[26] A. A. Abrikosov, Phys. Rev. B **60**, 4231 (1999).
[27] W. Zhang, R. Yu, W. Feng, Y. Yao, H. Weng, X. Dai, and Z. Fang, Phys. Rev. Lett. **106**, 156808 (2011).
[28] S. Lee, J. In, Y. Yoo, Y. Jo, Y. C. Park, H.-J. Kim, H. C. Koo, J. Kim, B. Kim, and K. L. Wang, Nano Lett. **12**, 4194 (2012).
[29] A. Sulaev, P. Ren, B. Xia, Q. H. Lin, T. Yu, C. Qiu, S.-Y. Zhang, M.-Y. Han, Z. P. Li, W. G. Zhu, Q. Wu, Y. P. Feng, L. Shen, S.-Q. Shen, and L. Wang, AIP Adv. **3**, 032123 (2013).
[30] V. D. Das and D. Karunakaran, Phys. Rev. B **39**, 10872 (1989).

[31] Y.-P. Gu, R. Cui, Z.-L. Zhang, Z.-X. Xie, and D.-W. Pang, J. Am. Chem. Soc. **134**, 79 (2012).
[32] A. Sahu, A. Khare, D. D. Deng, and D. J. Norris, Chem. Commun **48**, 5458 (2012).
[33] C.-N. Zhu, P. Jiang, Z.-L. Zhang, D.-L. Zhu, Z.-Q. Tian, and D.-W. Pang, ACS Appl. Mater. Interfaces **5**, 1186 (2013).
[34] M. D. Banus and M. C. Finn, J. EIectrochem. Soc. **116**, 91 (1969).
[35] M. Lee, T. F. Rosenbaum, M.-L. Saboungi, and H. S. Schnyders, Phys. Rev. Lett. **88**, 066602 (2002).
[36] Z. Zhao, S. Wang, H. Zhang, and W. L. Mao, Phys. Rev. B **88**, 024120 (2013).
[37] B. Yuan, Q. Tao, X. Zhao, K. Cao, T. Cui, X. Wang, and P. Zhu, Rev. Sci. Instrum. **85**, 013904 (2014).
[38] D. Santamaría-Pérez, M. Marqués, R. Chuliá-Jordán, J. M. Menendez, O. Gomis, J. Ruiz-Fuertes, J. A. Sans, D. Errandonea, and J. M. Recio, Inorg. Chem. **51**, 5289 (2012).
[39] J. Zhang, C. Liu, X. Zhang, F. Ke, Y. Han, G. Peng, Y. Ma, and C. Gao, Appl. Phys. Lett. **103**, 082116 (2013).
[40] M. D. Banus, Science **147**, 732 (1965).
[41] We notice that some early literatures have reverse definitions of $\alpha$ and $\beta$ phases. In this work $\alpha$ and $\beta$ phases are defined in the beginning to be consistent with most recent publications.
[42] B. H. Toby, J. Appl. Crystallogr. **34**, 210 (2001).
[43] X. Xi, C. Ma, Z. Liu, Z. Chen, W. Ku, H. Berger, C. Martin, D. B. Tanner, and G. L. Carr, Phys. Rev. Lett. **111**, 155701 (2013).
[44] A. R. Oganov and C. W. Glass, J. Chem. Phys. **124**, 244704 (2006).
[45] A. R. Oganov, A. O. Lyakhov, and M. Valle, Acc. Chem. Res. **44**, 227 (2011).
[46] A. O. Lyakhov, A. R. Oganov, H. T. Stokes, and Q. Zhu, Comput. Phys. Commun. **184**, 1172 (2013).
[47] A. R. Oganov, C. W. Glass, and S. Ono, Earth Planet. Sci. Lett. **241**, 95 (2006).
[48] Y. Ma, M. Eremets, A. R. Oganov, Y. Xie, I. Trojan, S. Medvedev, A. O. Lyakhov, M. Valle, and V. Prakapenka, Nature (London) **458**, 182 (2009).
[49] A. R. Oganov, J. Chen, C. Gatti, Y. Ma, Y. Ma, C. W. Glass, Z. Liu, T. Yu, O. O. Kurakevych, and V. L. Solozhenko, Nature (London) **457**, 863 (2009).
[50] Q. Zhu, A. R. Oganov, and A. O. Lyakhov, Phys. Chem. Chem. Phys. **15**, 7696 (2013).
[51] Q. Zhu, D. Y. Jung, A. R. Oganov, C. W. Glass, C. Gatti, and A. O. Lyakhov, Nat. Chem. **5**, 61 (2013).
[52] G. Kresse and J. Furthmüller, Phys. Rev. B **54**, 11169 (1996).
[53] J. P. Perdew, K. Burke, and M. Ernzerhof, Phys. Rev. Lett. **77**, 3865 (1996).
[54] See Supplemental Material at http://link.aps.org/supplemental/10.1103/PhysRevB.89.180102 for details of the experiments and calculations, Rietveld refinement results, and metastable structure information.
[55] R. Jeanloz, Geophys. Res. Lett. **8**, 1219 (1981).
[56] D. L. Heinz and R. Jeanloz, J. Appl. Phys. **55**, 885 (1984).
[57] B. K. Godwal, S. Stackhouse, J. Yan, S. Speziale, B. Militzer, and R. Jeanloz, Phys. Rev. B **87**, 100101 (2013).
[58] R. Dalven and R. Gill, Phys. Rev. **159**, 645 (1967).
[59] V. M. Glazov, S. M. Memedov, and A. S. Burkhanov, Sov. Phys. Semicond. **20**, 263 (1986).
[60] A. Segura, V. Panchal, J. F. Sánchez-Royo, V. Marín-Borrás, V. Muñoz-Sanjosé, P. Rodríguez-Hernández, A. Muñoz, E. Pérez-González, F. J. Manjón, and J. González, Phys. Rev. B **85**, 195139 (2012).
[61] R. Vilaplana, O. Gomis, F. J. Manjón, A. Segura, E. Pérez-González, P. Rodríguez-Hernández, A. Muñoz, J. González, V. Marín-Borrás, V. Muñoz-Sanjosé, C. Drasar, and V. Kucek, Phys. Rev. B **84**, 104112 (2011).
[62] C. M. Fang, R. A. De Groot, and G. A. Wiegers, J. Phys. Chem. Solids **63**, 457 (2002).
[63] In our frameworks of calculation, it is not possible to include SOC combined with GW [M. Shishkin and G. Kresse, Phys. Rev. B **75**, 235102 (2007)]. We note that the inaccuracies from first-principles calculations may result in an overlap between the conduction band and valence band, which is as small as 0.1 eV.
[64] J. R. Ziman, *Principles of the Theory of Solids* (Cambridge University Press, Cambridge, 1972), p. 250.